Kovove Mater. 49 2011 107–117
DOI: 10.4149/km_2011_2_107

Solution heat treatment of plasma nitrided 15-5PH stainless steel Part I. Improvement of the corrosion resistance

P. C. Borges[1]*, L. A. Rocha[2,3]

[1]*Departamento Acadêmico de Mecânica (DAMEC), UTFPR, Campus de Curitiba, Av. Sete de Setembro, 3165, Curitiba, 80230-901, Paraná, Brasil*
[2]*CT2M – Centre for Mechanical and Materials Technologies, Campus de Azurém, 4800-058 Guimarães, Portugal*
[3]*Departmento de Engenharia Mecânica, Universidade do Minho, Campus de Azurém, 4800-058, Guimarães, Portugal*

Received 6 July 2010, received in revised form 1 December 2010, accepted 3 December 2010

Abstract

The results of the investigation on Solution Heat Treatment of Plasma Nitrided (SHTPN) precipitation-hardened steel 15-5 PH are presented. The layers have been obtained by the plasma nitriding process followed by solution heat treatment at different temperatures. The influence of the solution heat treatment after nitriding on the dissolution process of the nitrided layer has been considered. The nitrided layers were studied by scanning electron microscopy, X-ray microanalysis (EDX), and X-ray diffraction. Micro-hardness tests of the nitrided layers and solubilized nitrided layers have been carried out and interpreted by considering the processing conditions. It was found that high nitrogen austenitic cases could be obtained after SHTPN of martensitic precipitation-hardened steel (15-5PH). When Solution Heat Treatment (SHT) was performed at 1100 °C, some precipitates were observed. The amount of precipitates significantly reduced when the temperature increased. The EDX microanalysis indicated that the precipitate might be chromium niobium nitride. When the precipitation on the austenite phase occurred in small amount, the corrosion resistance increased in SHTPN specimens and the pit nucleation potential also increased. The best corrosion result occurred for SHT at 1200 °C.

K e y w o r d s: solution heat treatment (SHT), plasma nitriding (PN), precipitation-hardening stainless steel, 15-5PH, solution heat treatment of plasma nitrided (SHTPN), corrosion resistance

1. Introduction

The study of the properties of high nitrogen stainless steel is a subject of considerable interest in the scientific community. The fabrication methods and properties of high nitrogen stainless steel have been described in a large number of publications. It has been reported that the presence of nitrogen has a great influence on the properties of the stainless steel, such as higher strength, ductility, work hardening, toughness, good corrosion resistance, and reduced tendency to grain boundary sensitization [1]. These properties are interesting for chemical, aerospace, and nuclear industries, and in particular for applications in sea water systems. Besides, nitrogen is a strong austenite stabilizer and is thereby able to promote the stabilization of austenite surface layer in martensitic stainless steel or martensite surface layer in ferritic stainless steel [2].

The higher performance of high nitrogen stainless steel results from the presence of nitrogen in solid solution. Nitrogen, carbon, and boron increase the strength of austenitic stainless steel considerably more than substitutional elements; however, nitrogen is found to be more effective than any other element [1].

Many processes have been developed aiming to introduce nitrogen and consequently increase the corrosion resistance and improve the mechanical properties of stainless steel. Some of the most commonly used methods are DC plasma nitriding at low temperature [3–7] and ion implantation [8, 9]. Recently, High-Temperature Gas Nitriding (HTGN) or solution

*Corresponding author: tel.: +55 41 3310-4783; fax: +55 41 3310-4660; e-mail address: pborges@utfpr.edu.br

nitriding has been introduced as a method for adding nitrogen to stainless steel [10–12].

The researches of Larish et al. [3], Liang et al. [4], and Lin et al. [5] have pointed out that it is possible to introduce nitrogen in solid solution on the surface of stainless steel by plasma nitriding. It was also confirmed that owing to the high stability of chromium nitride, the nitrogen stays only in solid solution when the low temperature plasma nitriding is carried out [3–5]. Li et al. [7] verified that plasma nitriding of 316L stainless steel at 350 ℃ produced the S phase with a thickness of about 5 μm and a wear resistance five times higher than that in untreated condition. It was found that treatment at temperatures higher than 400 ℃ results in the formation of CrN precipitates. Xi et al. [6] investigated the AISI 420 martensitic stainless steel and observed that plasma nitriding at low temperature increased the microhardness of the steel whereas an increase in the nitriding temperature resulted in an increase of the effective case depth with a slight decrease in hardness of the nitrided case. Thus, plasma nitriding improves the wear and corrosion resistance of the AISI 420 steel, namely regarding the pitting potential which becomes higher when compared to the non-treated samples. The best results of wear and corrosion resistance were achieved on steels nitrided at 350 ℃. When the plasma nitriding temperature is above 450 ℃ the amount of α_N phase decreases or completely disappears and CrN is formed which consequently results in the depletion of Cr in the solid solution of stainless steel. The CrN phases prevent the formation of a dense and continuous oxide film on the surface. This way, the corrosion resistance of AISI 420 stainless steel decreases as the nitriding temperature increases from 350 ℃ to 550 ℃.

Plasma Immersion Ion Implantation (PIII) can be used to obtain high nitrogen stainless steel layers. Abreu et al. [8] studied the effect of nitrogen implantation with an acceleration voltage of 150 keV and an implanted dose to saturation of 4×10^{17} ions cm^{-2} on AISI 304L stainless steel. The implanted N^+ ions penetrated about 140 nm while the maximum concentration was located at about 70 nm. The electrochemical behaviour indicates a clear improvement of the corrosion resistance in alkaline and chloride-containing media for the implanted specimens. Ma et al. [9] used the elevated temperature PIII process which combines conventional ion implantation and diffusion and results in a change of the element distribution and microstructure in the implanted layer. By these processes, a layer thickness of about 2 μm can be obtained, which is about one order of magnitude thicker than the layer thickness implanted at room temperature.

In HTGN, atomic nitrogen is absorbed at the surface of a conventional stainless steel (austenitic, martensitic, ferritic-austenitic, or martensitic-ferritic) from an N_2 or N_2 + Ar gas atmosphere. The temperature range is usually between 1000 and 1200 ℃. HTGN allows obtaining high nitrogen cases (between 0.5 and 2 mm depth). Garzón and Tschiptschin [10] investigated the effect of HTGN on austenitic stainless steel (UNS S30403) and ferritic-austenitic duplex stainless steel (UNS S31803). They pointed out that the nitrogen content has a linear influence on the hardness. It was found that with 1.1 wt.% of nitrogen, the hardness of UNS S31813 increased from 270 to 390 HV. Sung et al. [11] examined the phase changes, nitride precipitation, heat treatment, hardness variations, and tempering effect of AISI 430 ferritic stainless steel after HTGN at 1050 ℃ and 1100 ℃ in a nitrogen gas atmosphere. They observed that the surface layer of the steel was changed to martensite + ferrite and Cr_2N at 1050 ℃, while martensite plus a rectangular type retained austenite were observed at 1100 ℃. At 1100 ℃, the depth of the martensite phase was 0.13 and 1.2 mm for treatments carried out for 15 min and 10 h, respectively. When the nitrogen-alloyed AISI 430 steel was tempered, an increase in hardness was observed owing to the precipitation of nitride (CrFe)N and a secondary hardening effect resulting in a maximum value at 450 ℃. Above 550 ℃, the coarsening effect of the nitrides decreased the hardness considerably. The HTGN treatment thus improved the corrosion resistance while the high density precipitation of Cr_2N deteriorated the corrosion resistance.

It was observed that the ion implantation and low temperature plasma nitriding could produce higher nitrogen content on the coating layer, usually between 10 and 20 wt.%. The layer thickness was about few microns for the PIII process, and up to ten micrometers in depth could be generated in the surface region near 400 ℃ or at lower plasma nitriding temperature. Moreover, HTGN could produce a thickness layer of about 1 mm and nitrogen content less than 1.2 wt.%.

In the present study, a new process was applied in an attempt to enhance the mechanical and electrochemical properties of the 15-5PH stainless steel. The process consists of the Solution Heat Treatment of Plasma Nitrided (SHTPN) specimens. Layers produced by Plasma Nitriding (PN) and Solution Heat Treatments (SHT) at different temperatures were studied. The corrosion behaviour of the SHTPN specimens was evaluated and a relationship between the corrosion behaviour and the depth of the nitrided layers was established and correlated with the microstructure.

2. Experimental method

2.1. Materials and treatment

Prismatic samples ($12 \times 24 \times 7$ mm^3) of 15-5PH stainless steel were obtained from a 300×300 mm^2

Table 1. Nominal chemical composition of 15-5PH stainless steel (wt.%)

Elements (wt.%)												
C	Si	Mn	P	S	Cr	Ni	Nb	Cu	Mo	Co	Al	Fe
0.024	0.382	0.43	0.024	0.002	14.5	4.43	0.24	3.6	0.17	0.05	0.04	balance

Table 2. Parameters for plasma nitriding treatment

Parameter	Sputter cleaning	Plasma nitriding
Temperature T (℃)	160 ± 15	510 ± 20
Pulse duration P_d (μs)	200 to 300	600 to 800
Pulse pause P_p (μs)	800 to 900	300 to 400
Voltage U (V)	400	500
Total pressure P (Pa)	200 ± 15	400 ± 20
Time t (h)	1	2
Treatment gas	H_2	80 % N_2 + 20 % H_2

stainless steel plate in a solution treated condition by cutting and grinding up to 1200 grit to achieve a fine surface finish ($R_a \sim 0.4$ μm). The nominal composition of the steel is shown in Table 1. This condition was identified as **S**.

2.1.1. SHTPN

Prior to the SHTPN, the specimens were immersed and sonicated in alcohol to remove all kinds of oil and dust. PN was carried out in a pulsed-DC glow discharge plasma system of 400 mm diameter. The wall of the reactor acts as the anode and the samples were positioned radially in the centre. The samples were placed on the cathode and heated by ionic bombardment. The temperature in two samples was measured using a K-type thermocouple. To minimize the thermal gradient, three polished walls of stainless steel were introduced in the reactor that acted as a radiation shield. The respective processing conditions are shown in Table 2. The reactor used was similar to that used by Borges et al. [13], Maliska et al. [14], Borges et al. [15] and Bernardelli et al. [16]. This condition was identified as **N**.

The nitrided samples were solution heat treated in order to obtain a stainless steel with a high surface concentration of nitrogen in solid solution. In an attempt to prevent oxidation, the samples were encapsulated under vacuum in quartz tubes prior to the solution heat treatment. The treatments were carried out at different temperatures (1100, 1200, and 1275 ℃) for one hour followed by cooling in water at room temperature. These conditions were identified as **NS1**, **NS2,** and **NS3,** respectively. To ensure the quenched efficiency, the quartz tube was broken on reaching the water. A schematic representation of the time-temperature cycle of SHTPN is provided in Fig. 1.

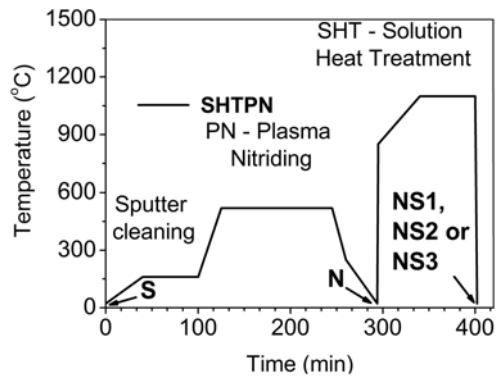

Fig. 1. Time-temperature cycle of SHTPN.

2.2. Characterization

The phase constituents and the microstructure of plasma nitrided layers and solubilized nitrided layers were characterized using Optical Microscopy (OM), Scanning Electron Microscopy (SEM), and Energy Dispersion Spectroscopy (EDS). Standard procedures were followed for preparing metallographic samples from transverse sections. Marble reagent was used as etchant (4 g of $CuSO_4$ + 20 ml of HCl + 20 ml of distilled water).

X-ray diffraction analysis (XRD) was carried out to determine the phase constituents in the samples using a Bruker D8 Discover Diffractometer with Cu Kα radiation and Ni-filter from 30° to 90° at a scan step size of 0.02° with 1 s step time.

Microhardness profile measurements (Vickers indenter, 100 gf) were carried out on the modified layers and on the matrix. The results of each point in the profile are the average of three measurements.

Open circuit potential (OCP) and potentiody-

Table 3. Quantity of removed material and region submitted to corrosion test

Region	Code	SHTPN studied condition		
		NS1	**NS2**	**NS3**
Outermost layer	P	10 to 20 μm	10 to 20 μm	10 to 20 μm
Austenite	A	95 to 110 μm	95 to 110 μm	95 to 110 μm
	B	195 to 210 μm	195 to 210 μm	195 to 210 μm
Martensite	C	350 to 365 μm	380 to 395 μm	490 to 510 μm

namic polarization tests were carried out in a three--electrode electrochemical cell in order to evaluate the corrosion resistance. A saturated calomel electrode was used as the reference and a platinum wire was used as the counter electrode. A GAMRY Reference 600 Potentiostat/Galvanostat equipment was used in the corrosion tests.

The OCP of the samples were recorded at 1 s intervals for 120 min. The potentiodynamic polarization tests were started at 100 mV below the OCP. All experiments were carried out at 22 ± 2 °C in a 3.5 % NaCl solution. The scan rate was 0.5 mV s^{-1}. The exposed area was 0.39 cm^2 in all the experiments. All tests were repeated at least three times.

To understand the influence of the nitrogen content and the distribution of phases on the corrosion behaviour in the SHTPN process, the measurements were performed at different depths. To achieve each depth, the samples were ground and the thickness of removed material was controlled using a micrometer. The depths selected for testing depended on the microstructure alterations after the SHTPN process. A code was used to identify the studied condition. The code was introduced in the beginning of the identification used for SHTPN studied condition (Table 3). Consequently, the corrosion result identified as BNS2 indicates: the corrosion resistance in a depth ranging between 195 and 210 micrometers of plasma nitrided specimens solubilized at 1200 °C.

The surface of the samples after corrosion tests was examined using a scanning electron microscope. The samples were cleaned with acetone and isopropyl alcohol in all stages prior to the corrosion tests and SEM examination.

3. Results and discussion

3.1. Nitriding

The aim of nitriding was to promote a high nitrogen nitrided case. This layer would be the source of nitrogen during the solution heat treatment. Five cycles of PN were carried out according to the parameters mentioned in Table 2. A typical cross-section of the plasma nitrided specimens is depicted in the microstructure presented in Fig. 2. It can be observed that a thick nitrided case is present. The layer appears slightly etched which implies that precipitation of nitrides may have occurred during the treatment. The average thickness of the nitrided case was about 66 ± 5 μm.

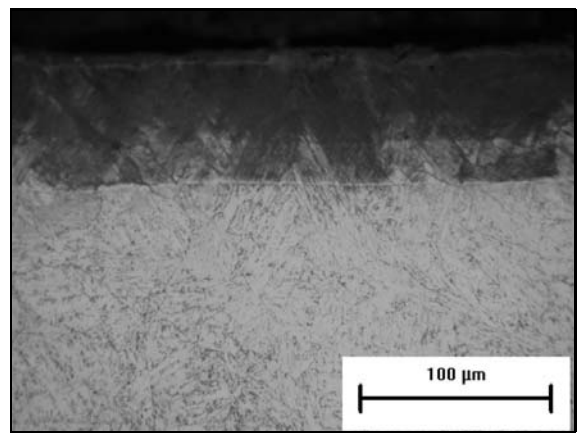

Fig. 2. OM micrograph of 15-5PH plasma nitrided at 520 °C for 2 h (**N**), marble reagent.

3.2. X-ray diffraction (XRD)

To ensure a clear understanding of the kind of phases formed in the surface layers of the nitrided samples, XRD patterns with Cu Kα radiation were obtained and compared to the un-nitrided sample as shown in Fig. 3. The sharp peaks on the XRD patterns correspond to the martensite (α') phase indicating the peaks in the un-nitrided or solution annealed samples (**S**). The XRD patterns of the nitrided (**N**) sample indicate that the main phase in nitrided samples is Fe_4N (γ') but some CrN appears in this plasma nitride condition. The presence of these phases is in accordance with the OM micrograph shown in Fig. 1. This result agrees with that reported by Bernardelli et al. in the study of the effect of simultaneous PN and ageing on the microstructure and corrosion resistance of 15-5 PH (Precipitation Hardening) stainless steel [16].

The XRD patterns of 1100 °C SHTPN and plasma nitrided samples (**N**) are shown in Fig. 4. It can

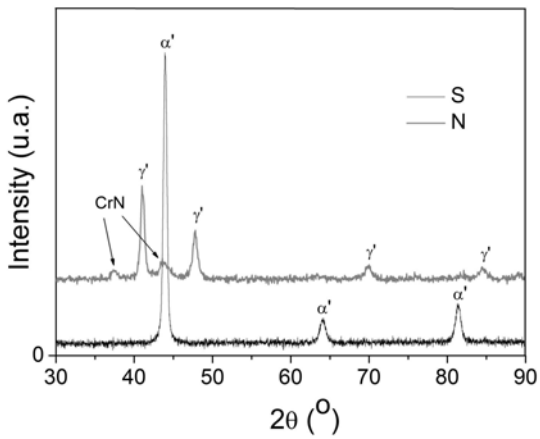

Fig. 3. X-ray diffraction patterns: un-treated sample (**S**) and nitrided sample (**N**).

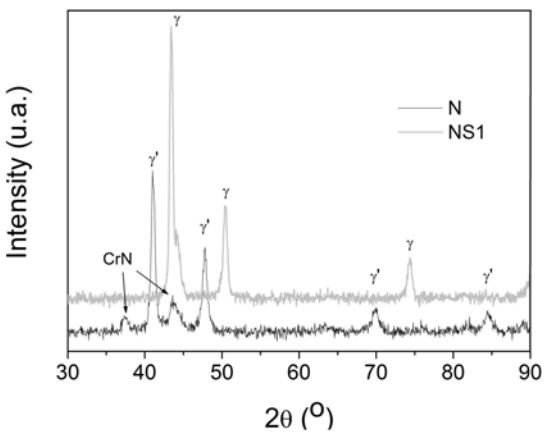

Fig. 4. X-ray diffraction patterns: plasma nitriding samples (**N**) and 1100 ℃ SHTPN (**NS1**).

be seen that all peaks of CrN and γ' phase disappeared after 1100 ℃ SHTPN. In fact, after 1100 ℃ SHTPN, the γ peaks and the weak α in the spectrum were detected. This α was considered to be martensite (α'). By comparing these results with the diffraction patterns of un-treated condition (**S**) shown in Fig. 3, it can be found that the microstructure changed from martensite (α') to austenite (γ) on the surface. These results indicate that SHT was effective on the dissolution of nitrides present in the plasma nitrided samples. No nitrided phase could be identified in 1100 ℃ SHTPN samples by this technique. Similar results were obtained for the samples treated at 1200 and 1275 ℃.

3.3. Microscopy

The typical microstructure of the SHTPN is shown in Fig. 5a. It can be observed that the SHTPN layer

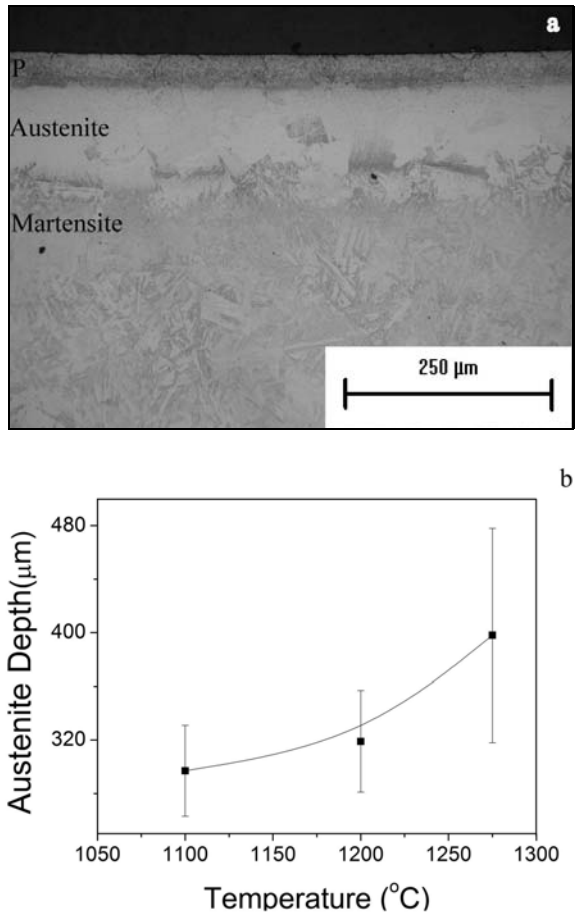

Fig. 5. Microstructure of 15-5PH SHTPN after different heat solution temperatures: a) OM micrograph of **NS1** (marble reagent), b) austenite depth × temperature.

has four principal regions:

– Pores, cracks and undissolved precipitates region with about 70 µm for all conditions (P region);
– an austenite region;
– high nitrogen martensite region;
– substrate.

The austenite depth taken from surface × temperature of SHTPN is shown in Fig. 5b. It can be seen that the austenitic region depths were mainly about 300, 320, and 400 µm of the depth for SHTPN specimens at conditions **NS1**, **NS2,** and **NS3**, respectively. Based on these results, it can be pointed out that the austenite depth increases when increasing the temperature for the conditions in this study. On the other hand it can be seen that the austenite depth dispersion increases as temperature increases. This occurs because when the temperature increases, there is a decrease in the surface nitrogen content (initial compound layer), in other words, it is not possible to maintain the surface nitrogen content as occurs in the HTGN process. Consequently, there is a deeper depth of layer, with a nitrogen content and an austen-

ite stability decrease. This way, the increase on solubility temperature and time should result in martensitic layers enriched with nitrogen. Other way to avoid the austenitic layers formation is to reduce the nitriding temperature and time, reducing the nitrogen content during the nitriding process.

By comparing Fig. 2 and Fig. 5a, it can be seen that the nitrided case for SHTPN was solubilized. As the austenite phase is stabilized by nitrogen content, it may be concluded that nitrogen is in solid solution [1, 10, 11]. Also, in the nitrided case region pores and cracks appear, and undissolved precipitates remain after solution heat treatment.

These rounded pores are probably related to the evolution of N(g) owing to the dissociation of nitrided phase. As the temperature increases to reach the temperature of the SHT, the stability of nitride phase decreases, thereby contributing to the dissociation into Fe, Cr, and N. The Cr and N diffuse into the steel matrix and result in the formation of solid solution. On the other hand, at temperatures used for SHT, nitrogen has a lower solubility in steel. Considering that the dissociation of nitride phase occurs more readily than the diffusion of nitrogen, this process results in the considerable evolution of N(g) because of low solubility of nitrogen in the steel matrix. According to Garzón et al. [17], the solubility of nitrogen in this temperature is less than 0.7 wt.% for steel with 22 wt.% of Cr, consequently for 15-5PH steel the nitrogen solubility limit should be lower. When the continuous dissociation on nitrided phase exceeds this critical concentration on nitrogen, the gas can no longer dissolve in the metal, and promotes the formation of pores. Consequently, the excess nitrogen remains trapped in the previous nitrided case and forms some pores in the P region.

The crack appears perpendicular to the surface. This effect is verified by the morphology of cracks indicated in Fig. 5a. These cracks are probably caused by the coalescence of pores in the P region during SHT. The directional propagation was favoured by the residual stresses in the nitrided layer, and consequently, the cracks were developed parallel to the direction of the residual stresses, generated by nitriding.

The cross section amplifications of SHTPN at 1100 and 1200 ℃ are shown in Fig. 6a and 6b, respectively (**NS1** and **NS2**). The microstructure of both conditions was predominantly austenite with a small quantity of precipitate and martensite. Three detailed regions can be seen in Fig. 6a which are: the region P, the austenite region at about 100 μm depth (identified by A), and the austenite region near 200 μm depth (identified by B). It is evident that no complete dissolution occurs in the regions P and A; however, in region B, a small quantity of precipitates as well as some martensite can be observed. The microstructure and details of the region P and the austenite region near 200 μm are shown in Fig. 6b. By comparing Fig. 6a,b, it can be concluded that there are more precipitates for SHTPN at 1100 ℃ than for SHTPN at 1200 ℃. The qualitative analysis on EDS shows that niobium, chromium, and nitrogen were higher on precipitates than in the matrix (see Table 4). This indicates that

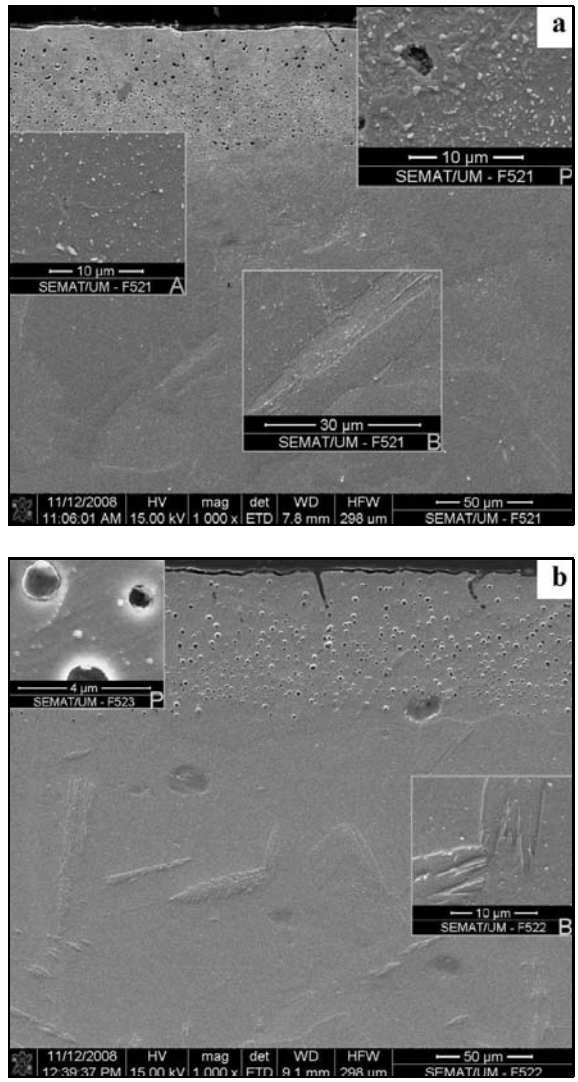

Fig. 6. SEM micrograph of 15-5PH SHTPN at different heat solution temperatures: a) 1100 ℃, b) 1200 ℃ (marble reagent).

Table 4. Nitrogen, niobium, and chromium composition in the matrix and precipitates

Point	Elements (wt.%)		
	N	Nb	Cr
Precipitated	8.78	3.15	20.09
Matrix	1.88	–	13.99

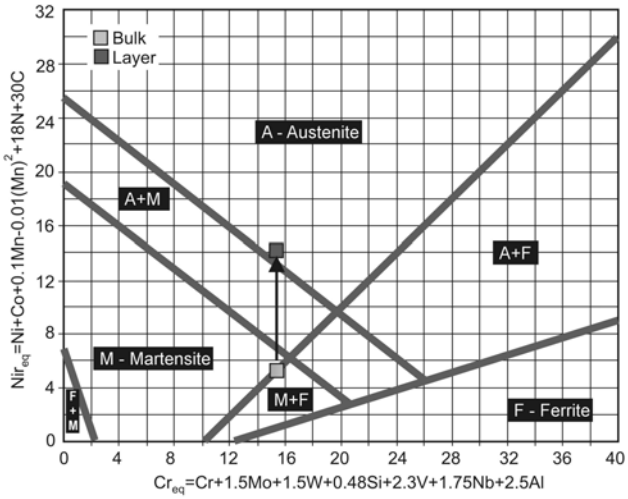

Fig. 7. Schaeffler's diagram reviewed by Speidel and Uggowitze (apud 10), showing the microstructure relationship between the bulk and the layer of SHTPN [10].

the precipitates can be chromium niobium nitrides. The sizes of the precipitates were about 0.4 μm for SHTPN at 1100 ℃ and about 0.2 μm for SHTPN at 1200 ℃. As expected, the size of the precipitates decreased with the increase in temperature. Generally high temperature treated materials suffer little distortion. Consequently, they are submitted to a finishing process. This way, the surface layer formed in the originally compound layer (after PN) can be removed after the SHTPN treatment.

The Schaeffler's diagram is a well-documented way to predict the phase composition for designing stainless steel alloys [10, 18]. In this study, the nitrogen content at the surface of SHTPN samples was estimated using the Schaeffler's diagram. The quantity of nitrogen necessary to stabilize the austenite phase was determined.

The Schaeffler's diagram reviewed by Speidel and Uggowitze (apud 10) is shown in Fig. 7. Point 1 (15.5; 5.2) is found using the composition of 15-5PH (**S**) and the equations for nickel equivalent (Ni_{eq}) and chromium equivalent (Cr_{eq}) shown on the Y and X axes. According to microstructural OM, SEM, and XRD analyses, it was proved that an austenitic region was formed on the surface of SHTPN samples. By considering the formation of austenite and by assuming that only the content of nitrogen changes during SHTPN, it can be said that the enrichment with this element establishes a new value to Ni_{eq}, changing the equivalent alloy coordinates from Point 1, relative to the original composition of 15-5PH, to Point 2 (15.5; 13.8). By applying the equation for nickel equivalent to estimate the nitrogen content relative to Point 2, a value of 0.56 % is found. Subsequently, this is the minimum nitrogen content necessary to stabilize the austenite

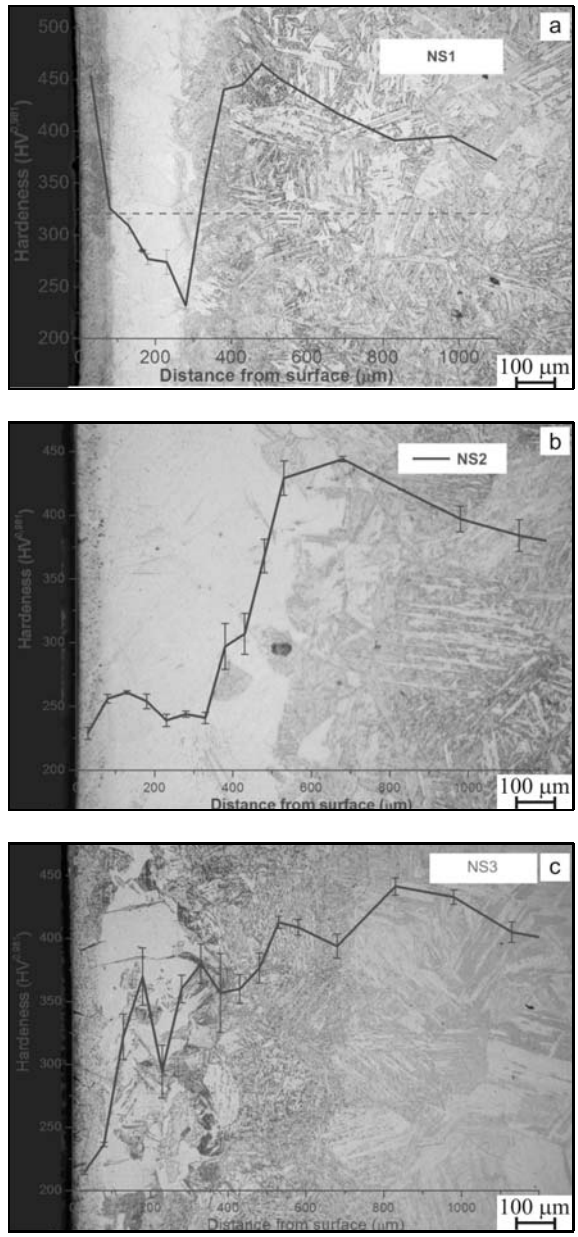

Fig. 8. Microhardness profiles average of SHTPN samples plotted on the cross-section microstructure: a) SHTPN at 1100 ℃ (**NS1**), b) SHTPN at 1200 ℃ (**NS2**), (c) SHTPN at 1275 ℃ (**NS3**).

phase. Probably the austenitic region has more than 0.56 % of nitrogen. By comparing this result with Fig. 5b, it can be concluded that the conditions used in this study (time and temperature of SHT) do not reduce the nitrogen content below the necessary values to destabilize the austenitic phase, and consequently, only traces of martensite occur in this region.

3.4. Cross-sectional hardness profile

The microhardness profiles average was plotted on

the cross-section microstructure of the samples. It is shown in Fig. 8a–c.

3.4.1. SHTPN at 1100°C

The microhardness profile of SHTPN samples at 1100 ℃ (**NS1**) has higher hardness on the surface (region P) and the hardness decreases with increasing the depth. This occurs because of the reduction of precipitates and nitrogen content. After 270 μm depth, the hardness sharply increases owing to the appearance of some martensite phase. The hardness value reaches its maximum to the Vickers hardness (465 HV) at about 480 μm and then decreases with depth owing to the reduction of nitrogen in the solid solution (Fig. 8a).

3.4.2. SHTPN at 1200°C

In the profile of SHTPN at 1200 ℃ (**NS2**) samples, the hardness increases from surface to the interface of the region P and the austenite region. This occurs due to a reduction in the pores. Subsequently, the hardness decreases from this interface to nucleus because of the reduction of nitrogen content in austenite. The hardness increases again near the interface between austenite and martensite because of the reduction of nitrogen content and consequent transformation of austenite to martensite. The hardness is the highest when martensite is 100 %. This happens at about 680 μm (441 HV); after this region, the hardness decreases again when the nitrogen content decreases (Fig. 8b).

3.4.3. SHTPN at 1275°C

The microhardness profile along the depth of the cross-section of SHTPN samples at 1275 ℃ (**NS3**) varies until the hardness value of 428 HV, at approximately 830 μm. This occurs because of the variation in the ratio of austenite to martensite in this region. After this position, the hardness decreases owing to the reduction of nitrogen content in the specimens (Fig. 8c).

3.5. Corrosion performance

The corrosion resistance for untreated (**S**), plasma nitrided (**N**), and SHTPN (**NS1, NS2,** and **NS3** at different depths) samples was investigated using the potentiodynamic polarization method in a solution of 3.5 % NaCl.

A series of polarization curves are shown in Figs. 9–13. The curves for untreated (**S**) and plasma nitrided (**N**) samples are represented in Fig. 9.

As seen in Fig. 9, the corrosion resistance of untreated sample is higher than that of nitrided samples (**N**). After nitriding, the samples present less noble potential and higher current density in the anodic region.

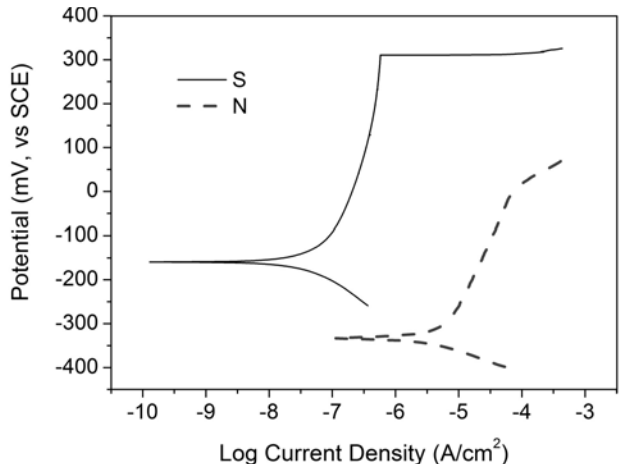

Fig. 9. Corrosion behaviour of 15-5PH, untreated (**S**), and nitrided (**N**) samples.

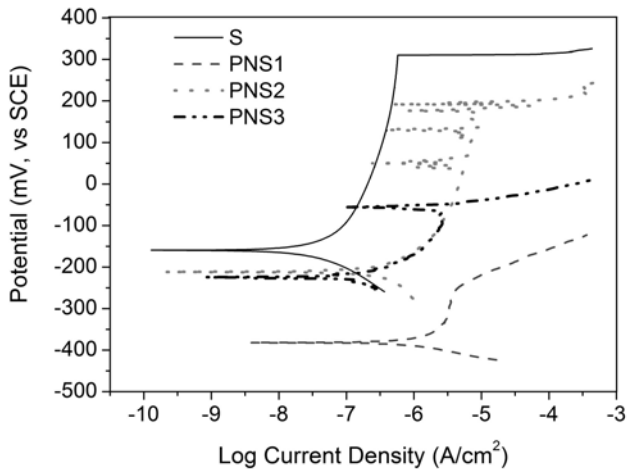

Fig. 10. Corrosion behaviour of 15-5PH, untreated (**S**), and superficial region (region P) of SHTPN (**PNS1**, **PNS2,** and **PNS3**) samples.

It was verified by XRD (Fig. 3) that nitrided samples have CrN precipitates and consequently there is depletion of Cr in the solid solution of nitrided layer. These results are responsible for low corrosion potentials as well as high corrosion rates.

The corrosion behaviour of untreated (**S**) and the region P of SHTPN samples at 1100 ℃ (**PNS1**), 1200 ℃ (**PNS2**), and 1275 ℃ (**PNS3**) is shown in Fig. 10. It can be seen that the region P exhibited the lowest corrosion resistance for all SHTPN conditions. The reason for less noble potential and higher current density in the anodic region might be explained on the basis of the increase in surface area owing to pores as well as owing to precipitates. It is interesting to note that the lowest values were obtained at lower treatment temperature for SHT. At this temperature, no

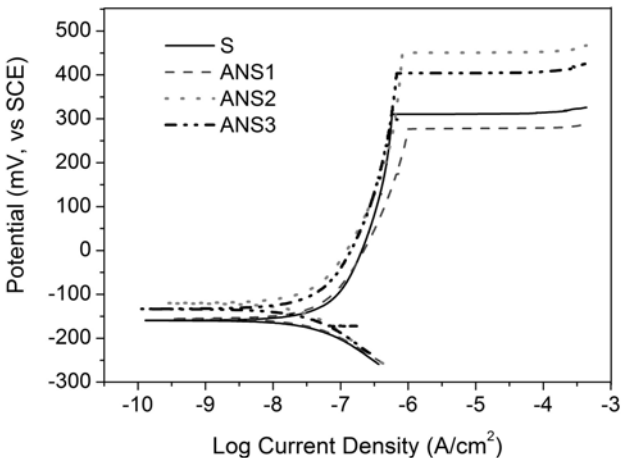

Fig. 11. Corrosion behaviour of 15-5PH, untreated (**S**), and austenite region (∼ 100 μm) of SHTPN (**ANS1**, **ANS2,** and **ANS3**) samples.

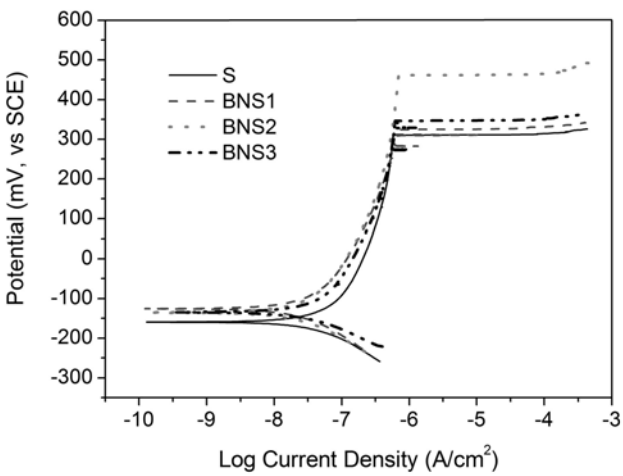

Fig. 12. Corrosion behaviour of 15-5PH, untreated (**S**), and austenite region (∼ 200 μm) of SHTPN (**BNS1**, **BNS2,** and **BNS3**) samples.

complete dissolution of nitrides was found to occur, despite the presence of a large number of precipitates (see Fig. 6a). When a high temperature of SHT was used, the polarization curves showed a tendency to passivity, and the current density for these points was similar to that of untreated samples (**S**). The heterogeneity decrease with the increase in temperature is shown in Fig. 6a,b; consequently, with the increase in temperature, the pit nucleation potential – E_{pit} (corresponding to a sudden rise in current, when pits start to form) also increases.

The corrosion behaviours of untreated (**S**) and austenite region (∼ 100 μm) of SHTPN (**ANS1**, **ANS2,** and **ANS3**) samples are compared in Fig. 11. It can be seen that the SHT samples treated over 1200 ℃ present better corrosion behaviour, especially the pit nucleation potential. The pit nucleation potential for samples treated at 1100 ℃ presents the lowest values. The observation under SEM strengthens the idea of the presence of precipitates in the surface layer as shown in the micrographs of Fig. 6a.

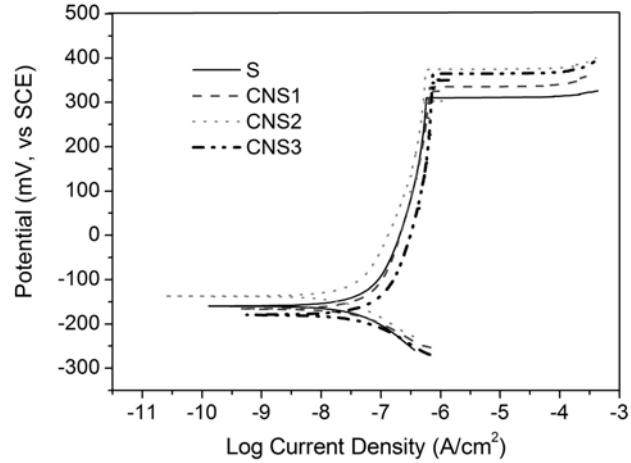

Fig. 13. Corrosion behaviour of 15-5PH, untreated (**S**), and martensite region (from 350 to 510 μm) of SHTPN (**CNS1**, **CNS2,** and **CNS3**) samples.

The corrosion behaviours of untreated (**S**) and austenite region (∼ 200 μm) of SHTPN (**BNS1**, **BNS2,** and **BNS3**) samples are compared in Fig. 12. It can be seen that all SHTPN samples present better corrosion behaviour, especially pit nucleation potential and anodic current. The pit nucleation potential for samples treated at 1200 ℃ presents the best results. It is believed that the austenite is more homogeneous at 1200 ℃ than the samples solubilized at 1100 ℃ when considering precipitates, and is more homogeneous than at 1275 ℃ when considering the presence of martensite phases. On the basis of this observation, it may be concluded that these heterogeneities are responsible for reducing the influence of high nitrogen content on the pit nucleation potential. Other consideration was that austenite formed at 1200 ℃ can have more nitrogen in solid solution than at 1275 ℃.

The corrosion behaviours of 15-5PH, untreated (**S**), and martensite region (from 350 to 510 μm) of SHTPN (**CNS1**, **CNS2,** and **CNS3**) samples are compared in Fig. 13. For this depth again, the best result was obtained for 1200 ℃ SHTPN samples with highest pit nucleation potential and lower anodic current density. For the other conditions, the pit nucleation potential was better than that obtained for the untreated condition; however, the current density was similar, if not lower.

The analyses carried out in Figs. 9 to 13 indicate that the lowest corrosion rates were obtained for SHTPN at 1200 ℃ on 100 μm (**ANS2**). On the other

hand, this condition showed the best Corrosion Rate (CR) and E_{pit} results for all depths except for the region P, where the surface generated poor results for both parameters. It was also observed that the pit nucleation potential was not evident for plasma nitrided samples (**N** in Fig. 9).

The corrosion resistance of stainless steels is owing to the thin and tenacious oxide film formed on the surface. It has been reported in the previous studies that the thickness of this film is about 1–4 nm; it consists of mainly Cr_2O_3 phase which leads to high corrosion resistance, and the durability of this oxide film is as important as its thickness and homogeneity [19]. In this study, it was observed that the encountered corrosion types were pitting corrosion. In accordance with results of Baba et al. [20] and Rotinick et al. [21], it can be mentioned that the nitrogen dissolved into the bulk during corrosion transformed into NH_4^+. This suggests that NH_4^+ consumes H^+ in the interface and decreases the pH; it also controls the pit nucleation and promotes the repassivation. Consequently, the role of dissolved nitrogen in the steel increases the repassivation capacity and increases the pit nucleation potential.

Garzon et al. [2] studied cavitation erosion resistance of a high temperature gas nitrided (HTGN) UNS S31803 duplex stainless steel, in substitute ocean water and verified that the nitrogen rich austenitic layer formed on the surface presented cavitation erosion resistance 24.5 times lower than the mass loss rate of an UNS S30403 SS solution treated. This way it can be considered that even though the low hardness, this layer can present excellent results in wear applications. On the other hand, increasing the solutioning time or temperature, or reducing the thickness of the layer formed during the PN, it can be obtained only martensitic layer with high hardness. These researches will be investigated next.

4. Conclusions

This study has examined the changes in microstructure, hardness variation, and the corrosion resistance as a result of PN and different temperatures of solution heat treatment of the 15-5PH stainless steel. The following conclusions have been made:

The strong affinity between nitrogen and Cr enables the permeation of nitrogen through 15-5PH stainless steel.

The nitrogen content on the surface layer changes the sample surface into austenite plus traces of martensite. The thicknesses of these layers are 300, 320, and 430 µm for SHTPN at 1100, 1200, and 1275 ℃, respectively.

SHTPN improves the corrosion resistance in the solution of 3.5 % NaCl for all conditions.

The effect of nitrogen on the corrosion resistance is to increase the pit nucleation potential.

Acknowledgements

The authors would like to acknowledge the support of the CT2M, Univ. do Minho, Portugal, Prof. Aloisio Schuitek, who machined the specimens, and CNPq, Brasil.

References

[1] SIMMONS, J. W.: Mater. Sci. Eng., *A 207*, 1996, p. 159. doi:10.1016/0921-5093(95)09991-3
[2] GARZÓN, C. M.—THOMAS, H.—SANTOS, J. F.—TSCHIPTSCHIN, A. P.: Wear, *259*, 2005, p. 145.
[3] LARISCH, B.—RUSKY, B. U.—SPIES, H. J.: Surf. Coat. Technol., *205*, 1999, p. 116.
[4] LIANG, W.—BIN, X.—ZHIWEI, Y.—YAQIN, S.: Surf. Coat. Technol., *130*, 2000, p. 304. doi:10.1016/S0257-8972(00)00713-1
[5] LIN, J. F.—CHEN, K. W.—WEI, C. C.—AI, C. F.: Surf. Coat. Technol., *197*, 2005, p. 28. doi:10.1016/j.surfcoat.2004.07.105
[6] XI, Y.—LIU, D.—HAN, D.: Surf. Coat. Technol., *202*, 2008, p. 2577. doi:10.1016/j.surfcoat.2007.09.036
[7] LI, C. X.—BELL, T.: Corros. Sci., *46*, 2004, p. 1527. doi:10.1016/j.corsci.2003.09.015
[8] ABREU, C. M.—CRISTÓBAL, M. J.—MERINO, P.—NÓVOA, X. R.—PENA, G.—PÉREZ, M. C.: Electrochim. Acta, *53*, 2008, p. 6000. doi:10.1016/j.electacta.2008.03.064
[9] MA, X.—JIANG, S.—SUN, Y.—TANG, G.—SUN, M.: Surf. Coat. Technol., *201*, 2007, p. 6695. doi:10.1016/j.surfcoat.2006.09.030
[10] GARZÓN, C. M.—TSCHIPTSCHIN, A. P.: Revista Matéria, *10*, 2005, p. 502.
[11] SUNG, J. H.—KONG, J. H.—YOO, D. K.—ON, H. Y.—LEE, D. J.—LEE, H. W.: Mater. Sci. Eng., *A 489*, 2008, p. 38. doi:10.1016/j.msea.2007.11.078
[12] BERN, H.—SIEBERT, S.: ISIJ International, *36*, 1996, p. 927.
[13] BORGES, P. C.—MARTINELLI, A. E.—MUZART, J. L. R.—KLEIN, A. N.—FRANCO, C. V.: Mater. Sci. Forum, *299–300*, 1999, p. 286. doi:10.4028/www.scientific.net/MSF.299-300.286
[14] MALISKA, A. M.—OLIVEIRA, A. A. M.—KLEIN, A. N.—MUZART, J. L. R.: Surf. Coat. Technol., *141*, 2001, p. 128. doi:10.1016/S0257-8972(01)01016-7
[15] BORGES, P. C.—MARTINELLI, A. E.—FRANCO, C. V.: Mat. and Corrosion, *55*, 2004, p. 594. doi:10.1002/maco.200303784
[16] BERNARDELLI, E. A.—BORGES, P. C.—FONTANA, L. C.—FLORIANO, J. B.: Kovove Mater, *48*, 2010, p. 115. doi: 10.4149/km_2010_2_105
[17] GARZÓN, C. M.—TSCHIPTSCHIN, A. P.: Mater. Sci. Eng. A, *441*, 2006, p. 230.
[18] RAWERS, J. C.: J Mater Sci, *43*, 2008, p. 3618. doi:10.1007/s10853-008-2576-3
[19] MILOŠEV, I.—STREHBLOW, H. H.: Electrochim. Acta, *48*, 2003, p. 2767.

[20] BABA, H.—KODAMA, T.—KATADA, Y.: Corrosion Science, *44*, 2002, p. 2393. doi:10.1016/S0010-938X(02)00040-9

[21] ROTNIK, U.—TANDLER, M.—VEHOVAR, A.—VEHOVAR, L.: Kovove Mater., *41*, 2003, p. 213.